

## In vitro and in silico studies of nitrobenzamide derivatives as potential anti-neuroinflammatory agents

Seda Savranoglu Kulabas, Ferah Comert Onder, Yakup Berkay Yılmaz, Adem Ozleyen, Serdar Durdagi, Kader Sahin, Mehmet Ay & Tugba Boyunegmez Tumer

To cite this article: Seda Savranoglu Kulabas, Ferah Comert Onder, Yakup Berkay Yılmaz, Adem Ozleyen, Serdar Durdagi, Kader Sahin, Mehmet Ay & Tugba Boyunegmez Tumer (2019): In vitro and in silico studies of nitrobenzamide derivatives as potential anti-neuroinflammatory agents, Journal of Biomolecular Structure and Dynamics, DOI: [10.1080/07391102.2019.1684368](https://doi.org/10.1080/07391102.2019.1684368)

To link to this article: <https://doi.org/10.1080/07391102.2019.1684368>

 View supplementary material [↗](#)

 Accepted author version posted online: 23 Oct 2019.

 Submit your article to this journal [↗](#)

 View related articles [↗](#)

 View Crossmark data [↗](#)

## LETTER TO THE EDITOR

### **In vitro and in silico studies of nitrobenzamide derivatives as potential anti-neuroinflammatory agents**

Seda Savranoglu Kulabas<sup>1</sup>, Ferah Comert Onder<sup>2</sup>, Yakup Berkay Yılmaz<sup>1</sup>, Adem Ozleyen<sup>1</sup>, Serdar Durdagi<sup>3\*</sup>, Kader Sahin<sup>3</sup>, Mehmet Ay<sup>2\*</sup>, Tugba Boyunegmez Tumer<sup>4\*</sup>

<sup>1</sup>Graduate Program of Biomolecular Sciences, Institute of Natural and Applied Sciences, Çanakkale Onsekiz Mart University, 17020 Çanakkale, Turkey.

<sup>2</sup>Natural Products and Drug Research Laboratory, Department of Chemistry, Faculty of Science and Art, Çanakkale Onsekiz Mart University, 17020 Çanakkale, Turkey.

<sup>3</sup>Computational Biology and Molecular Simulations Laboratory, Department of Biophysics, School of Medicine, Bahçeşehir University, 34353 Istanbul, Turkey

<sup>4</sup>Department of Molecular Biology and Genetics, Faculty of Science and Art, Çanakkale Onsekiz Mart University, 17020 Çanakkale, Turkey.

\*E-mails: [mehmetay17@gmail.com](mailto:mehmetay17@gmail.com) (MA, chemical synthesis), [serdardurdagi@gmail.com](mailto:serdardurdagi@gmail.com) (SD, in silico part), [tumertb@comu.edu.tr](mailto:tumertb@comu.edu.tr) (TBT, bioactivity studies)

### List of Abbreviations

|                        |                                    |
|------------------------|------------------------------------|
| <b>AD</b>              | Alzheimer's diseases               |
| <b>ALS</b>             | Amyotrophic lateral sclerosis      |
| <b>APP</b>             | Amyloid precursor protein          |
| <b>ARE</b>             | Antioxidant response element       |
| <b>BBB</b>             | Blood brain barrier                |
| <b>CNS</b>             | Central nervous system             |
| <b>CO</b>              | Carbon monoxide                    |
| <b>COX</b>             | Cyclooxygenase                     |
| <b>DMEM</b>            | Dulbecco's Modified Eagle's Medium |
| <b>DMSO</b>            | Dimethyl sulfoxide                 |
| <b>FBS</b>             | Fetal bovine serum                 |
| <b>Fe<sup>2+</sup></b> | Free ferrous iron                  |
| <b>HO-1</b>            | Hemeoxygenase                      |

|                               |  |
|-------------------------------|--|
| <b>IFD</b>                    | Induced fit docking  |
| <b>iNOS</b>                   | Inducible nitric oxide synthase                              |
| <b>KEAP1</b>                  | Kelch-like ECH-associated protein 1                          |
| <b>LPS</b>                    | Lipopolysaccharides  |
| <b>MCC</b>                    | Matthews correlation coefficient                             |
| <b>MD</b>                     | Molecular docking and molecular dynamics                     |
| <b>MS</b>                     | Multiple sclerosis   |
| <b>MTT</b>                    | 3-(4,5-Dimethylthiazol-2-yl)-2,5-diphenyltetrazolium bromide |
| <b>NF<math>\kappa</math>B</b> | Nuclear factor- $\kappa$ B                                   |
| <b>NO</b>                     | Nitric oxide   |
| <b>NO<sup>+</sup></b>         | Nitrosonium ion  |
| <b>NO<sup>-</sup></b>         | Nitroxyl radical   |
| <b>NQO1</b>                   | NADPH:quinoneoxido-reductase I                               |
| <b>Nrf2</b>                   | Nuclear factor-2 erythroid related factor-2                  |
| <b>ONOO<sup>-</sup></b>       | Peroxynitrite  |
| <b>PARP</b>                   | poly ADP-ribose polymerase                                   |
| <b>PBS</b>                    | Phosphate buffered saline                                    |
| <b>PD</b>                     | Parkinson's diseases   |
| <b>PPI</b>                    | Protein-protein interaction                                  |
| <b>QSAR</b>                   | Quantitative structure-activity relationships                |
| <b>RMSE</b>                   | Root mean squared error                                      |
| <b>RNOIs</b>                  | Reactive nitrogen intermediates                              |
| <b>SEM</b>                    | Standard error of mean                                       |
| <b>SOD</b>                    | Superoxide dismutase   |
| <b>SP</b>                     | Standard precision   |
| <b>TP</b>                     | Tanimoto prioritization                                      |
| <b>XP</b>                     | Extra precision  |

## INTRODUCTION

Neurodegenerative diseases are functional central nervous system (CNS) disorders that commonly characterized by the progressive deterioration of behavioral, cognitive and motor skills. Chronic neuroinflammation has been defined as common underlying thread for many neurodegenerative disorders including Alzheimer's and Parkinson's diseases (AD and PD, respectively), Multiple Sclerosis (MS), Amyotrophic Lateral Sclerosis (ALS), and even psychiatric illnesses such as depression. In recent years, it has become evident that gut microbiota can promote chronic low-grade inflammation and neuroinflammation through mechanisms involving increased exposure of the host to harmful bacterial products particularly to lipopolysaccharides (LPS) (Tse 2017). Systemic LPS and APP activate macrophages and microglia cells releasing variety of cytotoxic proinflammatory mediators. Among these effectors, particular attention has been paid to nitric oxide (NO) and its metabolic byproducts in mediating cytotoxicity and neurotoxicity in the last decade. In activated macrophages and microglia cells, inducible nitric oxide synthase (iNOS) produce micromolar concentrations of NO, which then reacts with oxygen and reactive oxygen species (ROS) including superoxide anions to form very reactive nitrogen intermediates (RNOIs), particularly peroxynitrite ion (Tse 2017). RNOIs may result in S-nitrosylation and nitrotyrosination of proteins that may finally lead to conformational changes (i.e., deformation) and modifications of their functional activities. Misfolding of Tau proteins in AD patients and nitrotyrosination of alpha-synuclein and Tau in PD and AD cases, respectively are two important hallmarks of neurodegeneration (Steinert, Chernova et al. 2010).

Besides protein deformation, NO and its secondary byproducts exert their cytotoxic and neurotoxic effects through several different mechanisms. In the center of all these processes strong and highly reactive free radical properties of these chemicals stand. Anomalous overproduction of RNOIs may damage DNA, which could lead to over activation of poly ADP-ribose polymerase (PARP) and cause neuronal ATP depletion and ultimately death. NO and peroxynitrite interact with iron containing enzymes and interfere with the cellular iron homeostasis, and irreversibly inhibit the activity of complexes I and II in mitochondrial electron transport chain, ATP synthase, aconitase and creatine kinase, thus disrupting mitochondrial energy production (Steinert, Chernova et al. 2010, Tse 2017). This also presents another reason for cellular ATP depletion, which is followed by neuronal death. NO

and peroxynitrite together can also reduce the cellular level of antioxidants such as ascorbic acid, plasma thiols and inhibit antioxidant enzymes such as glutathione peroxidase, NADPH quinoneoxido-reductase (NQO1).

The brain is very sensitive organ to cellular oxidative and nitrosative stress, which are two interconnected processes under inflammatory conditions because of its high lipid content, oxygen consumption capacity and presence of redox active metal ions such as Cu and Fe. Therefore, increased oxidant conditions and failures of antioxidant defense system by aberrant NO signaling are among the prerequisites for neurodegenerative diseases. Keeping redox homeostasis in brain is highly vital for preventing oxidative stress induced neuronal damage. Nuclear factor-2 erythroid related factor-2 (Nrf2) is prominent signaling molecule in cytoprotective defense system regulating inflammation to prevent neuronal death caused by activated macrophages and microglia cells. Upon oxidative/nitrosative stress stimuli, Nrf2 dissociates from Keap1 and translocates into the nucleus where it trans-activates antioxidant response element (ARE)-encoding genes including phase II detoxifying enzymes such as NQO1 and Glutathione S-transferases (GSTs) and antioxidant defense enzymes like superoxide dismutase (SOD) and catalase (Tumer, Yılmaz et al. 2018). The transcriptional repressions of iNOS, COX-2, proinflammatory cytokines and NF- $\kappa$ B in microglia, astrocytes and blood brain barrier (BBB) endothelial cells following Nrf2 activation have been well established. Therefore, NO inhibitors and Nrf2 activators may serve as effective multitarget pharmacological agents against inflammation elicited by APP and LPS.

The present study has been undertaken to investigate potent lead compounds to block induction of iNOS and at the same time to induce the cytoprotective enzyme system under inflammatory condition by using *in vitro* and *in silico* analyses. The benzamide functional group is an important pharmacophore present in the structures of therapeutically important marketed drugs such as moclobemide, remoxipride and tiapride, which are used in the treatment of some neurological disorders. In our previous studies, a series of nitro substituted benzamide derivatives with potent LPS induced NO inhibitory activity were reported (Tumer, Onder et al. 2017). Continuing our interest in understanding the biological implications of the structural characteristics in benzamide derivatives, we studied with eight nitro benzamide derivatives (Figure 1). Moreover, in this work, binary disease quantitative structure-activity relationships (QSAR) models, molecular docking and molecular dynamics (MD) simulations and pharmacokinetic approaches as well as toxicity QSAR models were integrated in order to

investigate their therapeutic predictions, structural/dynamical properties as well as pharmacokinetic profiles.

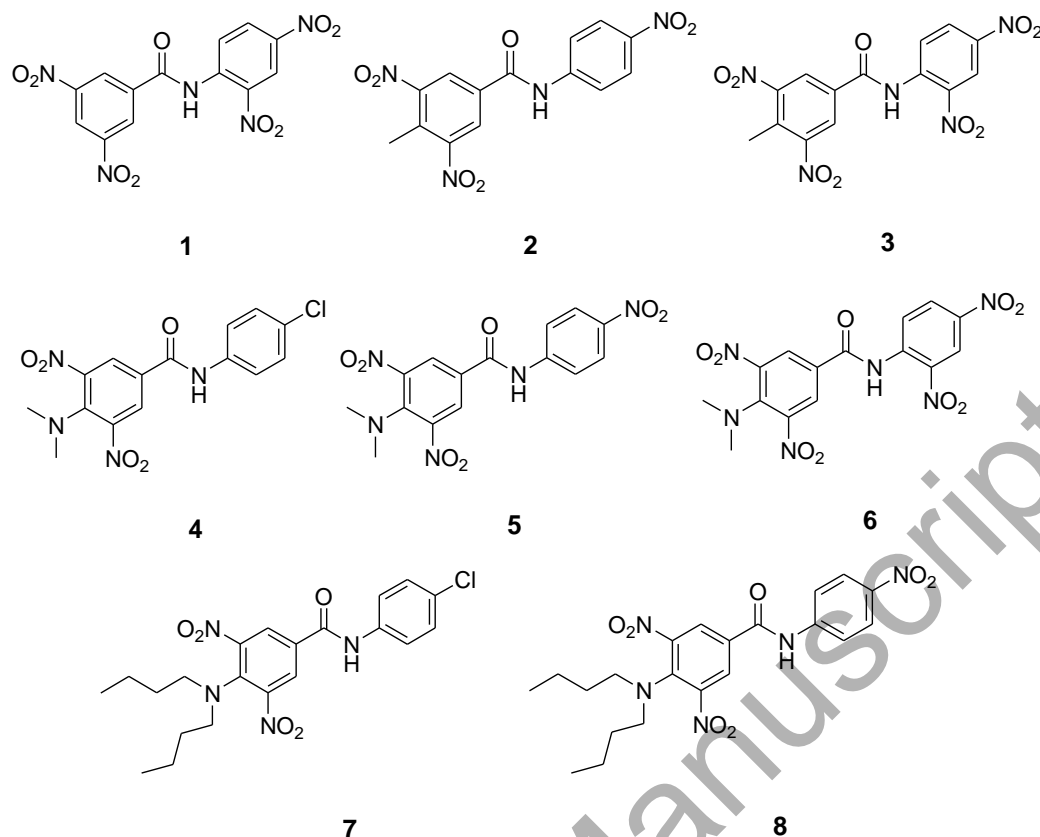


Figure 1. Structures of the synthesized compounds

## MATERIALS AND METHODS

### Chemicals.

Dulbecco's Modified Eagle's Medium (DMEM) high glucose, Dulbecco's Modified Eagle's Medium F-12 Nutrient Mixture, 3-(4,5-Dimethylthiazol-2-yl)-2,5-diphenyltetrazolium bromide (MTT), sodium pyruvate, methanol, N, N-methylenbisacrylamide, dimethyl sulfoxide, phosphate buffered saline (PBS) and lipopolysaccharide (LPS) from *Escherichia coli* O55:B5 were purchased from Sigma-Aldrich Chemical (St Louis, Missouri, USA). TRIzol®, Trypsin-EDTA, fetal bovine serum (FBS), horse serum, nuclear and cytoplasmic extraction reagents NE-PER™ (Thermo Scientific, Rockford, IL, USA), PureLink® RNA mini kit, cDNA8 synthesis kit, DNase I, TaqMan® PCR Master Mix, , TaqMan® Probe iNOS, TaqMan® Probe  $\beta$ -Actin, TaqMan® Probe Nrf2, TaqMan® Probe HO-1 and TaqMan® Probe NQO1 were purchased from Life Technologies, Thermo Fisher Scientific

(Waltham, MA USA). Protease/phosphatase inhibitor cocktail (100X) were obtained from Cell Signaling Technology (Leiden, Netherlands).

Immobilon Classico Western HRP substrate (WBLUC0500) and anti-iNOS (sc-650), were purchased from Santa Cruz Biotechnology (Bergheimer, Heidelberg, Germany), anti-Nrf2 (NBP1-32822) was purchased from Novus (Abingdon Oxon, England).

### **General procedure for the synthesis of aromatic amide substituted compounds (1-8).**

The compounds were synthesized from various 3,5-dinitrobenzoic acid and different aniline derivatives by using DCC and DMAP at room temperature for 12-24 hours with high and mild yields and also, 4-dibutylamino-3,5-dinitrobenzoic acid as starting material was obtained from 4-chloro-3,5-dinitrobenzoic acid and dibutylamine in methanol at reflux conditions for 3 h for the synthesis of compounds *N*-(4-Chlorophenyl)-4-(dibutylamino)-3,5-dinitrobenzamide (**7**) and *N*-(4-Nitrophenyl)-4-(dibutylamino)-3,5-dinitrobenzamide (**8**). The structures of the studied compounds are given in Scheme 1. Detailed synthesis methods and spectral analysis of these compounds were described in our study and its supplementary material (Güngör, Önder et al. 2019).

### **Cell Culture and sample treatment.**

Murine RAW macrophages (RAW264.7, ATCC®TIB-71™) cell line was kind gift of Dr. Ilya Raskin (Rutgers University, NJ, USA). It was routinely cultured and maintained in 100 U/mL penicillin, 100 µg/mL streptomycin, and 10% fetal bovine serum (FBS) containing high glucose DMEM. Murine SIM-A9 microglia (ATCC® CRL-3265™) cell line was purchased from American Type Culture Collection (ATCC). They were routinely propagated in DMEM/F-12 supplemented with 100 U/mL penicillin, 100 µg/mL streptomycin, 10% fetal bovine serum (FBS) and 2% horse serum. Both cells were incubated at 37 °C in humidified air containing 5% CO<sub>2</sub>. For treatments, cells were plated at a density of 4x10<sup>5</sup> or 1.5x10<sup>6</sup> cells/mL in 24-well or 6 well plates, respectively in phenol red free media containing 10% FBS and then incubated with or without LPS (1 µg/mL) and compounds (1-8) or with positive control (1400W) as triplicate for 24 h. Compounds were dissolved in 10% dimethyl sulfoxide (DMSO) and final concentration of DMSO was 0.1% in each well. All biological experiments were repeated at least three times, and the data were represented as mean values (means ± SD).

### **Cell viability assay (MTT).**

The effects of compounds on cell viability was examined at different doses (10, 20, 50, 100  $\mu\text{M}$ ) by using MTT assay as described previously (Tumer, Onder et al. 2017).

### **Nitric oxide production assay.**

RAW264.7 macrophage and SIM-A9 microglia cells were seeded to 24-well plates with the  $4 \times 10^5$  cells/mL density in phenol red free media containing 10% FBS and then cultured with or without LPS (1  $\mu\text{g/mL}$ ) and various doses of compounds as triplicate for 24 hours. Released NO concentration was assayed by using Griess reaction method as previously described (Tumer, Yilmaz et al. 2018).

### **Gene expression analyses by quantitative PCR.**

The gene expression levels of iNOS, Nrf2, HO-1, NQO1 and  $\beta$ -Actin (as a reference gene) were investigated quantitatively by using specific TaqMan® Gene Expression Assays (Thermo Scientific, Rockford, IL, USA). RAW264.7 macrophage and SIM-A9 microglia cells were seeded to 24-well plates at a density of  $4 \times 10^5$  cells/mL in phenol red free medium supplemented 10% FBS. Cells were simultaneously treated with 1  $\mu\text{g/mL}$  LPS and various doses of compound **1** and **3** and then incubated for 24 hours. Total RNA was isolated from cells by using Pure Link® RNA mini kit plus on-column DNase treatment according to manufacturer's specifications (Applied Biosystems, Foster City, CA). The protocol has been modified by using TRIzol for better quality of isolation and purification of RNA as previously described (Tumer, Onder et al. 2017).

### **Cell lysate preparation and Western blot analysis.**

RAW264.7 macrophage and SIM-A9 microglia cells were seeded to 6-well plates with the  $1.5 \times 10^6$  cells/mL density in phenol red free medium containing 10% FBS and then cultured with or without LPS (1  $\mu\text{g/mL}$ ) and various doses of **1** and **3** as triplicate for 6 hours. After treatments, cells were washed with PBS and cell lysis was extracted by using RIPA buffer to obtain total cell lysate. The cytoplasmic and nuclear fractions of cells were obtained by using nuclear and cytoplasmic extraction reagents NE-PER™ (Thermo Scientific, Rockford, IL, USA). The BCA protein assay kit (Thermo Scientific, Rockford, IL, USA) was performed to

quantify the protein content of the cell lysates which were then separated on a discontinuous buffer system including 4% stacking gel and 8.5% SDS-PAGE. The gel was subjected to Western blotting. Nitrocellulose membrane was incubated with iNOS, Nrf2, Lamin and  $\beta$ -actin primary antibodies (Santa Cruz Biotechnology, Santa Cruz, CA) overnight while shaking at 4 °C. The details of the procedure were carried out as previously described in the study of Tumer, Yilmaz et al. 2018.

### **Molecular docking calculations.**

Before the docking, both studied ligands and proteins were prepared in physiological conditions. The structures of studied compounds were sketched using Maestro molecular modeling package and 3D structures were first subjected to energy minimization. Then, LigPrep module of Maestro with OPLS3 forcefield were used to prepare the compounds. Epik was used to generate protonation states for molecules at pH 7.4. Crystal structures of the target proteins were retrieved from the Protein Data Bank, (PDB entries: 4NOS for iNOS and 2FLU for Keap1). The missing atoms of the proteins (i.e., hydrogen atoms) and missing (if any) side chain atoms were added and the water molecules within the catalytic domains were kept using protein preparation module of Maestro molecular modeling tool. The systems were assigned at a physiological pH by PROPKA, and finally in order to relax the protein, energy minimization was performed by the OPLS2005 forcefield method. The binding sites of the target proteins were defined based on the co-crystallized ligands and these sites together with the water molecules were considered as docking boxes in the simulations. The ions, small molecules that were used to help crystallization and water molecules that were not in the vicinity ( $> 5 \text{ \AA}$ ) of co-crystallized ligand were removed before the docking.

Algorithms used in the docking studies included Glide's standard precision (SP), extra precision (XP) and Induced Fit Docking (IFD) modules in Maestro with flexible ligand sampling. A receptor grid box was generated and certain amino acids were allowed to rotate their side chains to add flexibility to the used target. IFD method comprises 3 consequent stages, including (i) docking of the compounds while the receptor is rigid; (ii) refining the complex amino acids within  $5 \text{ \AA}$  of the ligand using Prime; (iii) finally redocking of the compounds using refined binding pocket.

### ***In Silico* Pharmacokinetic Studies.**

MetaCore/MetaDrug was used for analysis of therapeutic activity properties, pharmacokinetic properties and toxicity effects of compounds **1** and **3**. MetaCore/MetaDrug provides a comprehensive tool to analyze compounds and their biochemical and pharmacological behaviors in the field of drug design and development. MetaDrug uses the property of Tanimoto Prioritization (TP) to find the similarity between analyzed compounds and compound sets in the quantitative structure-activity relationships (QSAR) models based on elements found in the structure. Details of the method has been previously described in our recent paper (Kanan, Kanan et al. 2019).

### **Molecular Dynamics (MD) Simulations.**

The complexes were hydrated in the cubic box with explicit TIP3P water molecules that have 10 Å thickness from surfaces of protein. The MD simulations were performed by Desmond. The particle mesh Ewald method was used to calculate the long-range electrostatic interactions and a cut-off radius of 9 Å was used for both van der Waals and Coulombic interactions. Nose-Hoover thermostat and Martyna-Tobias-Klein protocols were used to adjust the temperature and pressure of the systems at 310 K and 1.01325 bar, respectively. The time-step was assigned as 2.0 fs. The default values were used for minimization and equilibration steps and finally 100-ns production run was performed for each simulation.

### **Statistical analysis.**

Statistical analyses were carried out by using GraphPad Prism 5 software. For the comparison of independent samples (group means), Student's t-test was used. Statistical significance was considered at  $p < 0.05$ . All experiments and analyses were repeated at least three times. Results were expressed as mean  $\pm$  standard error of mean (SEM).

## **RESULTS AND DISCUSSION**

### **Chemistry.**

In our previous study (Tumer, Onder et al. 2017), we showed the effectiveness of six different substituted aromatic amide compounds which include nitro functional groups at the different positions on the phenyl ring, thus, in this study, synthesized eight derivatives of aromatic amide compounds (**1-8**) that contain different functional groups such as  $-\text{NO}_2$ ,  $-\text{N}(\text{CH}_3)_2$ ,  $-\text{N}(n\text{-Bu})_2$ ,  $-\text{CH}_3$  and  $-\text{Cl}$  on both of their side rings, as prodrug for Ntr-based cancer therapies,

were examined to better understand the effect of pharmacophore groups and their iNOS enzyme inhibition characteristics.

According to structures of the compounds, the similar group effects on the same positions were observed within our previous and current studies. When the nitro groups exist at the -2,4 and -3,5 positions on the phenyl ring, we determined the increased activity results in *in vitro* analysis and this circumstance was compared with the known iNOS inhibitors like 1400W. Here, the compounds 3,5-dinitro-*N*-(2,4-dinitrophenyl)benzamide (**1**) and 4-methyl-3,5-dinitro-*N*-(2,4-dinitrophenyl)benzamide (**3**) were found as highly potent iNOS inhibitors due to their better electron withdrawing properties and mesomeric effects that suitable structural orientations of the nitro group on positions -2,4 and -3,5 at the binding pocket of the target structure. Similar behavior of nitro derivatives at the binding pocket of the iNOS has been shown in our previously reported study (Tumer, Onder et al. 2017).

Furthermore, compound **3** exhibited the lowest IC<sub>50</sub> (3.8 μM) value than compound **1** (5.8 μM) for NO production in the presence of the methyl group that shows electron donating properties on phenyl ring.

#### **Identification of the lead compounds: *In vitro* screening by NO inhibition.**

Among eight nitro benzamide derivatives, two compounds have been identified as promising lead compounds according to results obtained from NO inhibition assay in LPS induced RAW 264.7 macrophages. For each assay, a control (vehicle alone), and an induction control (1 μg/mL LPS) were used to set a baseline data. 1400W, a highly potent and selective iNOS inhibitor, was used as positive control in both experimental and docking studies. All tested compounds exhibited no cytotoxic effect (>90% cell viability-data not shown) on cells at 10 μM.

As shown in Figure 2, all compounds (**1-8**) were first screened for their effect on LPS induced NO production in RAW 264.7 macrophage cells at 10 μM. Among eight compounds, **1** and **3** showed potent effects-more than 50% inhibition- against NO production at 10 μM with inhibition rates of 81% and 52% respectively (p<0.05 for both). Therefore, **1** and **3** were selected as lead compounds and the rest of the experiments were carried out to identify their potency and mechanism of action as potential neuroprotective agents in LPS induced macrophages and microglia cells.

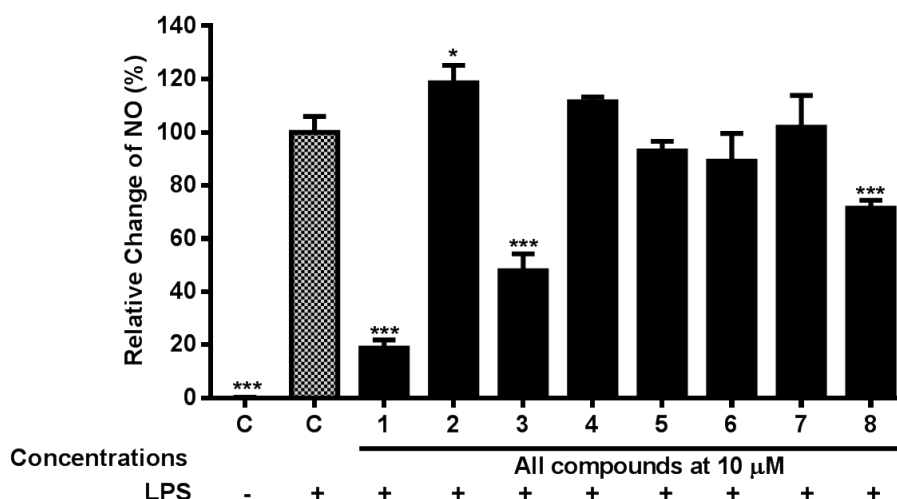


**Figure 2.** Screening of compounds at 10  $\mu\text{M}$  for inhibiting LPS-induced NO production in RAW 264.7 macrophage cells. The figure shows the mean results of the triplicate experiment for each treatment group. 1400 W: Positive control. C: Control. Each bar represents the mean  $\pm$ SEM, \* $p < 0.02$ , \*\*\* $p < 0.001$ .

### The effects of 1 and 3 on cell viability.

We performed MTT assay in both RAW 264.7 macrophage and SIM-A9 microglia cell lines to determine the concentrations at which 1 and 3 reveal no cytotoxic effects. As seen in Figure 3, treatment with 3 did not affect the cell viabilities in both cell lines up to highest tested concentration (100  $\mu\text{M}$ ). However, macrophage and microglia cell lines demonstrated slightly different sensitivity towards 1. While in macrophages for all tested doses cell viabilities were more than 80%, in SIM-A9 at 100  $\mu\text{M}$  the cell viability decreased slightly to 77.5 %.

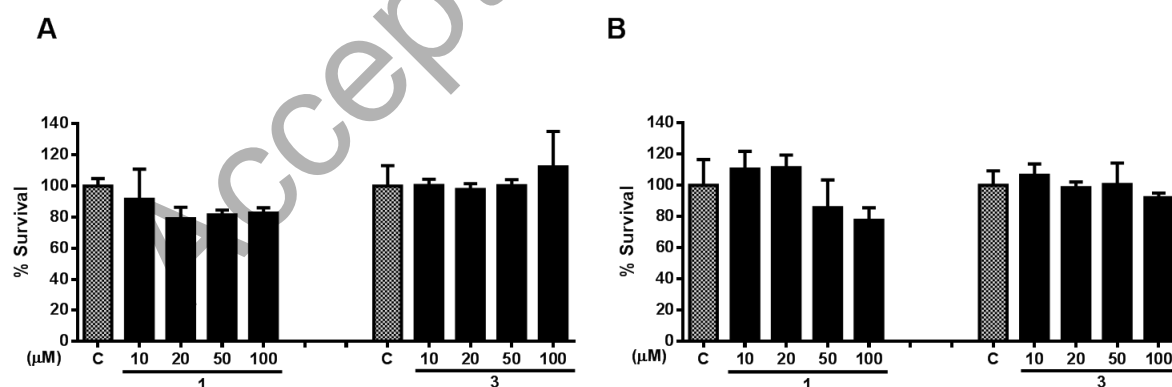


**Figure 3.** Effects of 1 and 3 on cell viability in (A) RAW 264.7 macrophage and (B) SIM-A9 microglia cell lines. The figure shows the mean results of the triplicate experiment for each treatment group. C: Control, \*\* $p < 0.05$ , \*\*\* $p < 0.001$ .

### **Effects of lead compounds on NO/iNOS signaling in LPS induced macrophage and microglia cells.**

Considerable evidence has shown that iNOS-derived NO secreted from microglia and macrophage cells is one of the major sources of cytotoxic mediators in brain. The reactions of NO with molecular oxygen, transition metals and superoxide result in the formation of potent oxidizing agents such as nitrosonium ion ( $\text{NO}^+$ ), nitroxyl radical ( $\text{NO}^-$ ), peroxynitrite ( $\text{ONOO}^-$ ), and many other secondary metabolites generated from these precursors with profound cytotoxic effects. The neurotoxic effect of NO and its byproducts may involve several mechanisms such as protein dysfunction through S-nitrosylation or tyrosine nitration, promoting apoptotic and necrotic cell death, direct DNA damage and/or inhibiting DNA repair mechanisms (Steinert, Chernova et al. 2010, Tse 2017). Elevated levels of nitrate and nitrite were detected in the cerebrospinal fluid of patients with MS and the cerebrospinal fluid concentration of these cytotoxic compounds was found to be correlated with the breakdown of the BBB (Thiel and Audus 2001). NO and peroxynitrite have been implicated in the pathogenesis of MS, AD and PD where NO was found to be neurotoxic to oligodendrocytes and neurons, and inhibited the mitochondrial respiratory chain (Thiel and Audus 2001). Therefore, iNOS has emerged as a functionally important source of oxidative/nitrosative brain injury. For this reason, pharmacologic inhibition of this enzyme is a rational approach in the prevention as well as treatment of various neurodegenerative diseases. Under pathological conditions, a known iNOS inhibitor, 1400W, stabilizes blood pressure but has a direct adverse effect on evoked potential amplitudes that does not appear in physiological conditions. Because of this effect, the interpretation of the effects on neurovascular coupling is limited; however, there was no clear positive effect. Thus, there is still some room for novel potent inhibitors of iNOS that have high binding affinity and specificity as well as with desired pharmacokinetic profiles. Therefore, targeted approaches to intervene NO/iNOS signaling pathway should be considered. In the present study, when both RAW 264.7 macrophages and SIM-A9 microglia cells were simultaneously treated with different concentrations of these two molecules (0.5-12  $\mu\text{M}$ ) and LPS (1  $\mu\text{g}/\text{mL}$ ), as seen in Figure 4, NO production was significantly inhibited in a dose-dependent manner.

The  $\text{IC}_{50}$  values of these two molecules were investigated for NO production and were resulted in 5.8  $\mu\text{M}$  for **1** and 3.8  $\mu\text{M}$  for **3**, which are comparable to  $\text{IC}_{50}$  of 1400W (1.84  $\mu\text{M}$ )

a selective and irreversible inhibitor of iNOS. In LPS-induced SIM-A9 microglia cells, same compounds gave slightly higher IC<sub>50</sub> values, which were found to be 6.1 μM for **1**, 10.8 μM for **3** and 2.2 μM for 1400W. Microglia cells are gaining remarkable interest in recent years due their role in different neurodegenerative and neurological disorders (Tse 2017). SIM-A9 cell line has been recently isolated glial culture from murine cerebral cortices (Nagamoto-Combs, Kulas et al. 2014). It is the first spontaneously immortalized microglial cell clone demonstrating major characteristics of cultured primary microglia and serves as a suitable model for the research studies of neuroinflammation when challenged with LPS or amyloid β. Since the establishment of this cell line as *in vitro* model is very recent, the number of research studies is also very limited, besides there is no study investigating any specific iNOS inhibitor on this cell line. Recently, NO inhibitory capacities of L-carnitine and vateriferol, a new resveratrol trimer, on SIM-A9 cell line have been reported (Gill, Raman et al. 2018, Samaradivakara, Samarasekera et al. 2018). Accordingly, L-carnitine inhibited LPS induced NO release at relatively high concentrations (Gill, Raman et al. 2018). When the L-carnitine concentration exceeds 5 mM, the rate of LPS induced NO inhibition could reach to 50%. Also, treatment of LPS-induced SIM-A9 cells with vateriferol at 14.7 and 73.6 μM resulted in a dose dependent significant inhibition, however, at both doses, the rate of inhibition could not reach to 50% (Samaradivakara, Samarasekera et al. 2018). Therefore, the inhibition potencies of **1** and **3** on NO/iNOS signaling at quite low micro molar ranges (3.8-10.8 μM) in both macrophages and microglia cells enable these two molecules promising as lead neuroprotective agents.

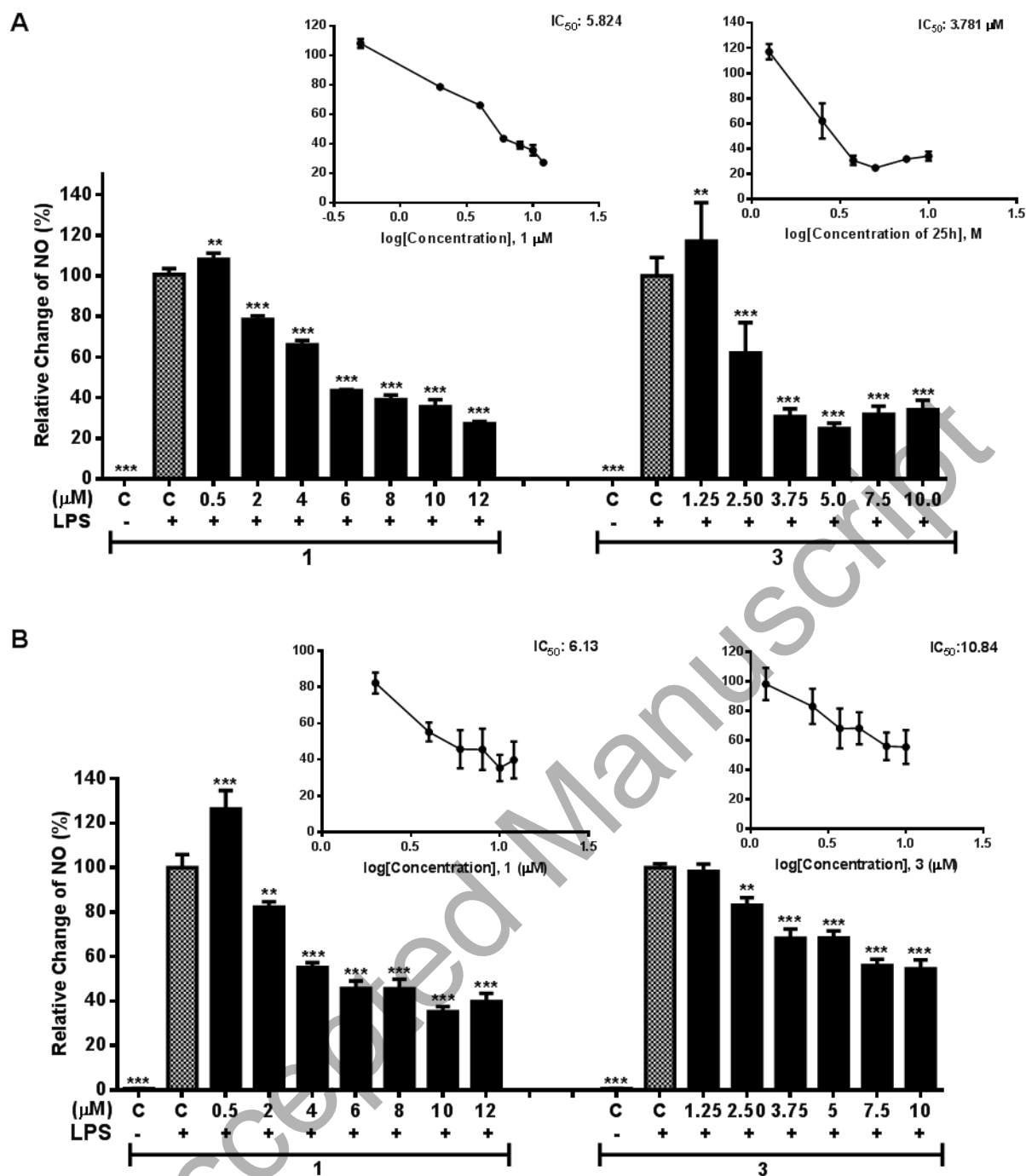


**Figure 4.** (A) Effect of **1** and **3** on NO production in LPS induced RAW 264.7 macrophage cells. (B) Effect of **1** and **3** on NO production in LPS induced SIM-A9 microglia cells. The cells were treated with LPS (except for negative control-C) and various doses of the **1** and **3**. The figures show the mean results of the triplicate experiment. C: Control. Each bar represents the mean  $\pm$ SEM, \*\*p<0.05 \*\*\*p<0.001.

iNOS is not expressed in normal brain but expression can be induced in microglia cells and macrophages only under pathological situation. The mechanism of induction involves transcription of mRNA and novel protein synthesis. In the pathogenesis of various neurodegenerative disorders such as MS, AD and PD, both iNOS protein and mRNA expressions were found to be markedly elevated in the active lesions of the patients' brain (Thiel and Audus 2001, Steinert, Chernova et al. 2010).

In the present study, treatment of RAW 264.7 macrophages and SIM-A9 microglia cells with **1** (5-20  $\mu$ M) resulted in substantial down regulations in both mRNA and protein levels of iNOS (Figure 5). In macrophages, compound **1** at 10 and 20  $\mu$ M suppressed LPS-induced iNOS mRNA level 56% and 69%, respectively as compared to LPS-induced control cells (Figure 5A). Similar to mRNA, iNOS protein expression also decreased 52% and 60% by **1** at 10 and 20  $\mu$ M, respectively. Compound **3** (10 and 20  $\mu$ M) in macrophages also suppressed LPS-stimulated iNOS expression significantly at both mRNA (72% and 62%, respectively) and protein levels (66% and 60%, respectively). Although, compound **3** resulted in significant suppression in both mRNA and protein levels of LPS induced microglia cells, the pattern of downregulation was not dose dependent and also it was not as potent as this seen in macrophages (Figure 5B). However, compound **1** at 10 and 20  $\mu$ M suppressed the LPS-induced iNOS expression at mRNA level 60% and 61%, respectively. Protein levels were also suppressed by 5, 10 and 20  $\mu$ M treatment of compound **1** dose dependently by 30%, 53% and 58%, respectively.

Therefore, potent inhibition and downregulation capacities of both compounds, particularly compound **3** on NO/iNOS signaling at three level of expression (activity, mRNA and protein levels) support potential anti-neuroinflammatory and neuroprotective effects of these compounds on degenerative disorders of CNS.

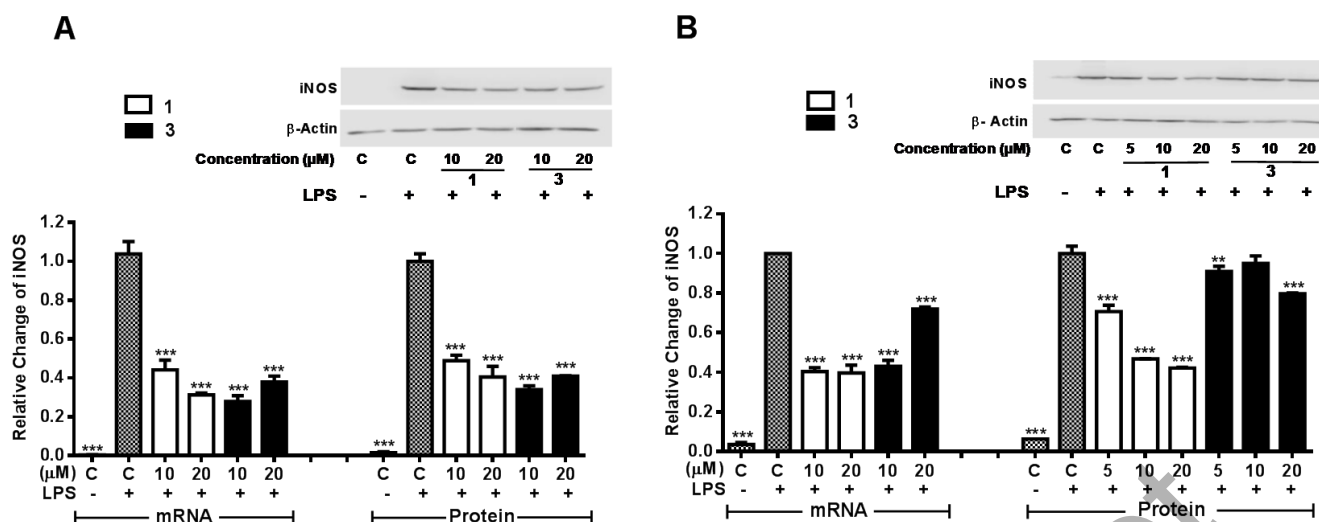


**Figure 5.** (A) Effect of **1** and **3** on iNOS mRNA and protein expression in LPS induced RAW 264.7 macrophage cells. (B) Effect of **1** and **3** on iNOS mRNA and protein expression in LPS induced SIM-A9 microglia cells. The cells were treated with LPS (except for negative control-C) and 5, 10 and 20  $\mu$ M doses of the **1** and **3**. The figures show the mean results of the triplicate experiment. C: Control. Each bar represents the mean  $\pm$ SEM, \*\*p<0.05, \*\*\*p<0.001.

### *In Silico* Investigation of Studied Compounds at the Binding Pocket of iNOS.

In order to investigate binding interactions of studied molecules, all eight nitro derivatives have been docked to the binding pocket of iNOS using Glide/SP, Glide/XP and Induced Fit (IFD) docking algorithms. Same docking protocol has been applied to the well-known iNOS inhibitor 1400W and Ronopterin as positive control compounds. Docking scores confirmed the potent molecules **1** and **3** (Table S1 of the Supporting Information). Docking scores also fits well with the experimental findings (i.e., compounds **1** and **3** shows promising binding interactions with the target enzyme but their  $IC_{50}$  values are slightly bigger than 1400W). When the top-docking poses of compounds **1** and **3** were superimposed, it can be seen that they have similar binding interactions with the target residues (Figure 6). Binding cavity for both compounds were formed with following residues: Glu377, Gln263, Ala282, Arg388, Tyr373, Trp372, Gly371, Arg266, Arg381, Val352, Pro350, Phe369 and Trp463. Compound 1400W has also similar binding cavity with the **1** and **3**. Salt bridge interaction and hydrogen bond were constructed with Glu377 for compound **1**. Corresponding interactions were formed

with Arg266, Gln263 and Glu377 for compound 3 (Figure 6). Glu377 also forms a salt bridge interaction with 1400W.

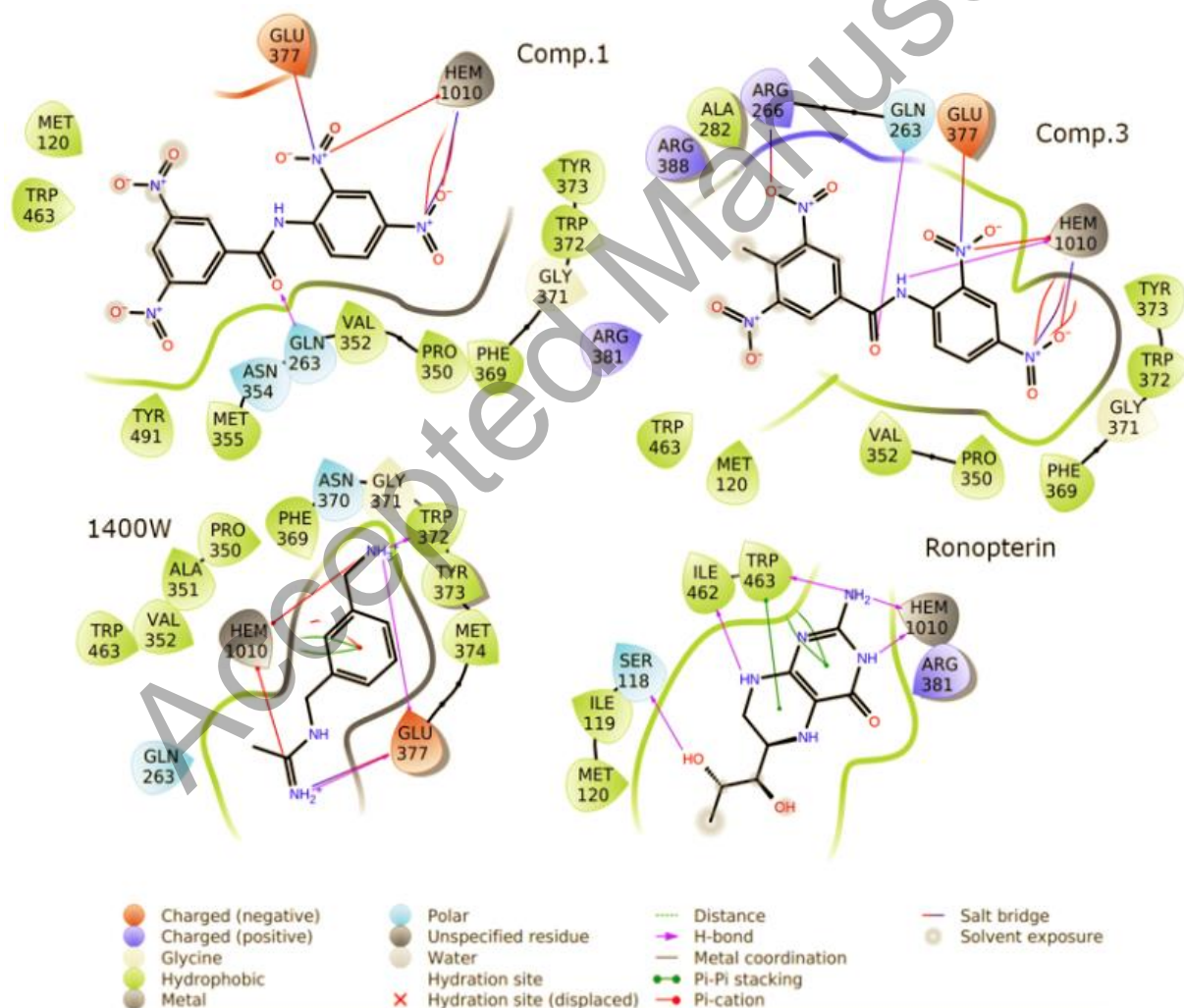
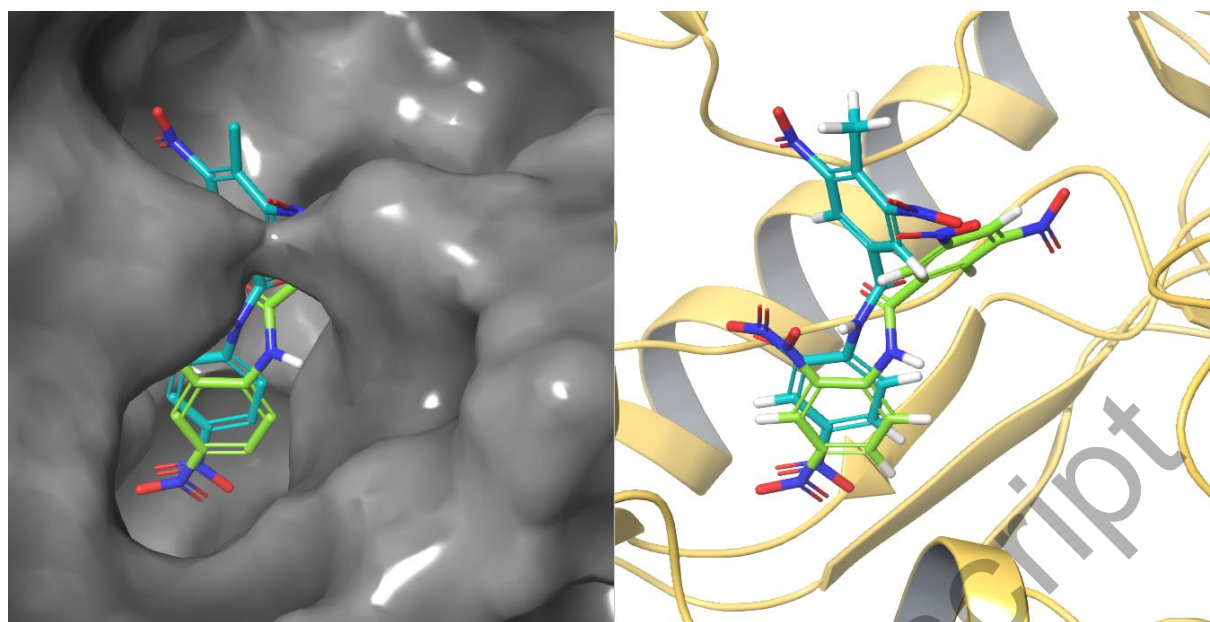


**Figure 6.** 2D and 3D ligand interaction diagrams of compounds **1** and **3** at the binding pocket of iNOS using top-docking poses (Glide/XP). Results were compared with positive control 1400W and Ronopterin.

Top-docking poses of compounds **1**, **3**, 1400W and ronopterin were used as initial structure and all-atom classical molecular dynamics (MD) simulations were performed in order to investigate time-dependent dynamics of both ligands and target atoms. Fluctuations of ligand at the binding pocket can be investigated by root mean square fluctuation (RMSF). Figure S1 at the supplementary information shows RMSF of iNOS based on C $\alpha$  atoms. Figure represents which regions of protein have higher mobilities compared to other parts. Especially regions of residue numbers 20-50, 70-80, 190-195 and 320-340 show higher mobility. Most mobile regions of ligand can be also monitored throughout the MD simulations. Ligand RMSF may give insights on how ligand fragments interact with the binding pocket residues and their entropic role in the binding event. So, translational (based on protein) and rotational (based on ligand itself) RMSF of ligand has been computed (considering only heavy atoms). Figure 7 shows rotational and translational RMSF of the compound **3**. It can be seen that especially atom numbers 15-19 and 20-22 at the ligand show higher translational motion during the simulations. The region of atom numbers 24-28 has higher rotational motion.

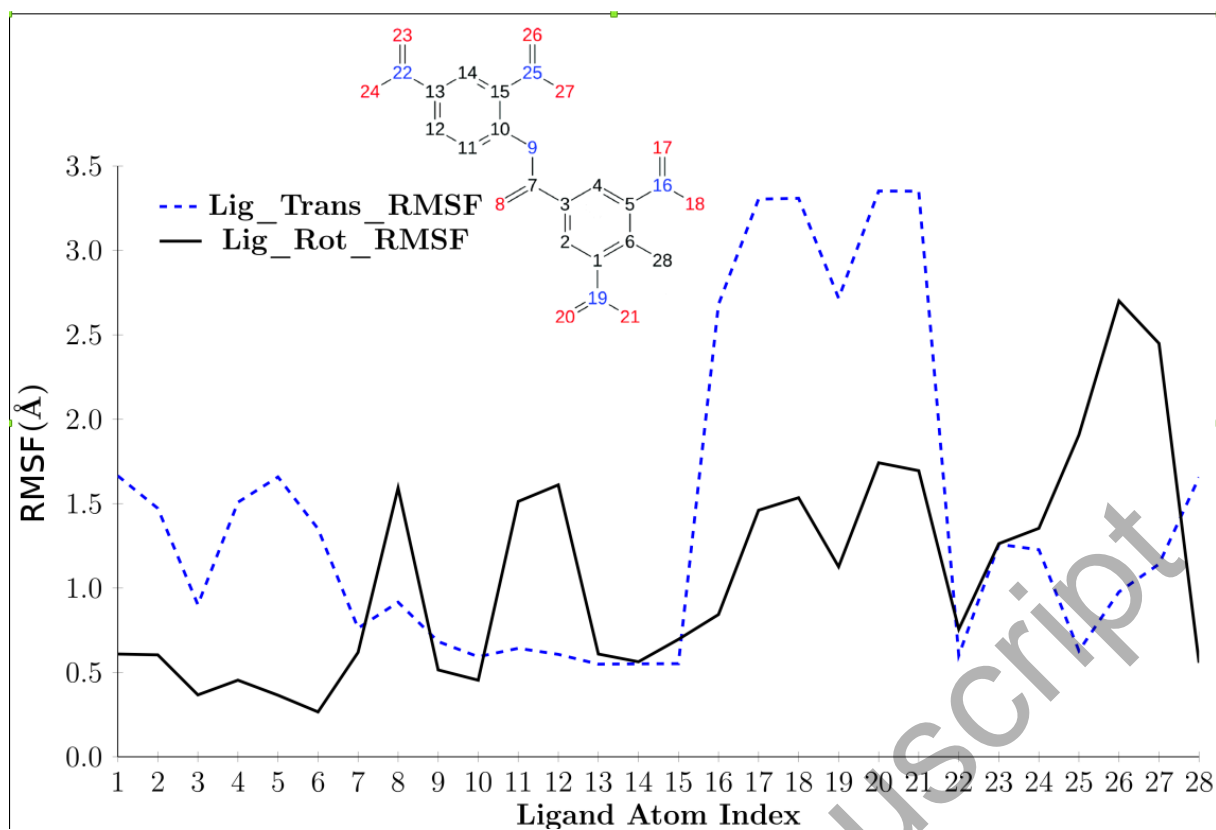


**Figure 7.** Translational and rotational RMSF of compound **3** at the binding pocket of the target.

Torsional profile of the compound **3** has been also investigated throughout the simulation (Figure S2). The figure summarizes the conformational changes of every rotatable bond at the compound **3**. Each torsional angle at the rotatable bond is accompanied by a radial and bar plots. Radial plots show the torsional angle changes during the simulations (the beginning of the simulation is in the center of the radial plot and the time evolution is plotted radially outwards).

Protein-compound **3** interactions have been monitored throughout the MD simulations. Figure 8 represents the crucial residues for the ligand contacts. It can be seen that especially Cys200, Gln263, Arg266, Val352, Asn354, Arg381 and Arg388 have higher interaction fractions with the ligand at the binding pocket. Similar analysis has been carried out for the 1400W and ronopterin it is found that especially Pro350, Val352, Trp372 and Glu377 have crucial roles in binding for 1400W (Figure S3) and Cys200, Gln263, Pro350, Gly371, Tyr373, Glu377, Asp382 for ronopterin (Figure S4).

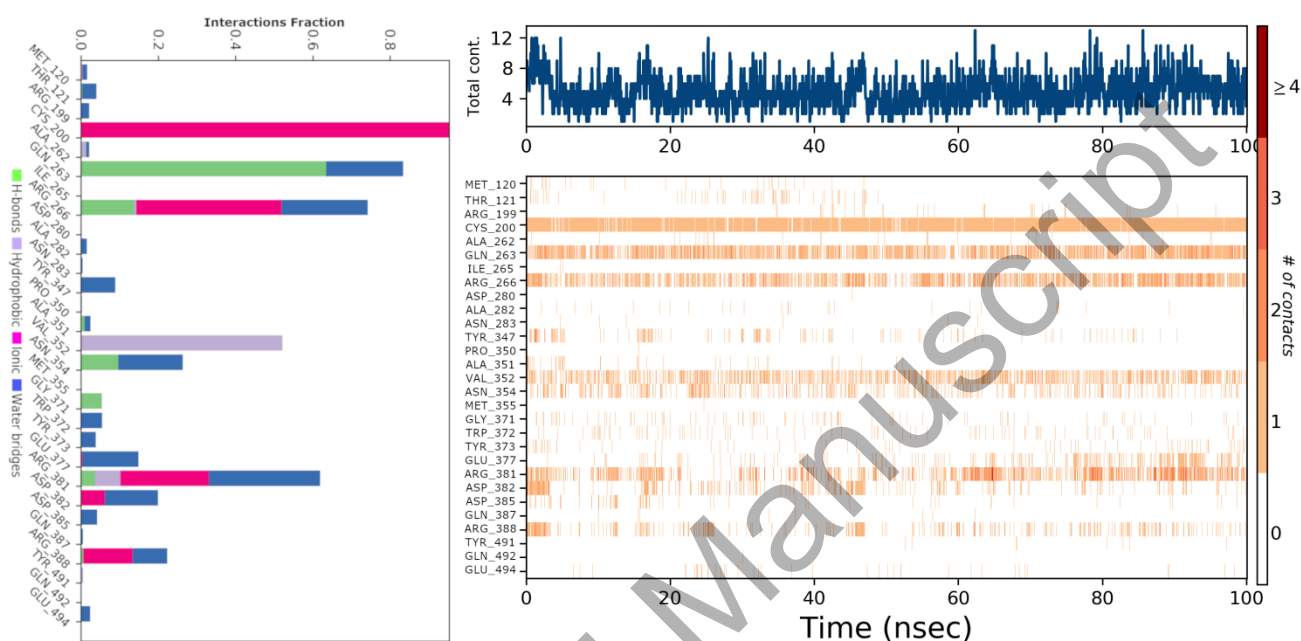


**Figure 8.** Protein-compound **3** contacts throughout the MD simulations.

MM/GBSA continuum solvation approach is well-defined method for estimating the free energy of binding of small ligands to a specific biological target (Shityakov, Sohajda et al. 2014, Shityakov, Roewer et al. 2017). Derived trajectory frames throughout the MD simulations were used in MM/GBSA calculations. MM/GBSA calculations were performed for compounds **1**, **3** as well as positive controls 1400W and Ronopterin. (Table S1) Results of selected compounds gave similar binding energies with positive controls.

Our computational investigation results showed that selected compounds (**1** and **3**) have similar interaction energy profiles with the two selected positive control compounds in this study.

### The effects of **1** and **3** on Nrf2 mRNA Levels and Its Transactivated Target Gene Expression.

Oxidative stress is accepted as crucial player in the pathogenesis of various chronic inflammatory diseases including neurodegenerative disorders. Nrf2 activators attenuate multiple pathogenic processes in which disruption of redox homeostasis and chronic inflammation coexist including various neurodegenerative disorders (Tumer, Yılmaz et al. 2018).

In the present work, we studied the effects of compounds **1** and **3** on the mRNA expression of Nrf2 and its downstream enzymes under inflammatory conditions in both macrophages and microglia cells. As shown by Figure 9, **1** at 10 and 20  $\mu$ M increased the mRNA expression of Nrf2 in a dose dependent manner both in macrophages (1.4-1.7 fold, respectively) and microglia cells (2.0-2.4 fold, respectively) as compared to control group. Treatment with **3**, resulted in very similar effects at same doses in macrophage (1.8 and 2.0 fold upregulation, respectively) and microglia cells (2.5 and 2.9 fold upregulation, respectively).

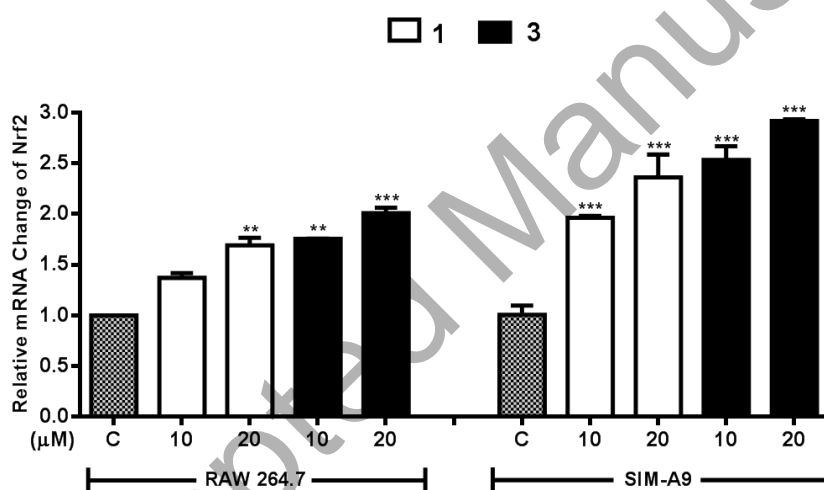


**Figure 9.** Effect of **1** and **3** on Nrf2 mRNA expression in LPS induced RAW 264.7 macrophage cells and SIM-A9 microglia cells. The cells were treated with LPS and 5, 10 and 20  $\mu$ M doses of the **1** and **3**. The figures show the mean results of the triplicate experiment. C: Control. Each bar represents the mean  $\pm$ SEM, \*\* $p$ <0.05, \*\*\* $p$ <0.001.

Both compounds **1** and **3** also resulted in a marked upregulation in the expression of NQO1 enzyme, a prototypic Nrf2 target in both LPS induced inflammation model of macrophage and microglia cells. In the present study, as presented in Figure 10, compound **1** at 10 and 20  $\mu$ M upregulated mRNA level of NQO1 3.2 and 10.1-fold in macrophages and 8.8 and 17.6-fold, respectively in microglia cells. Compound **3** at same doses resulted in more potent

increases which were 5.3 and 10.6-fold in macrophages and 14.8 and 26.3-fold, respectively in microglia cells.

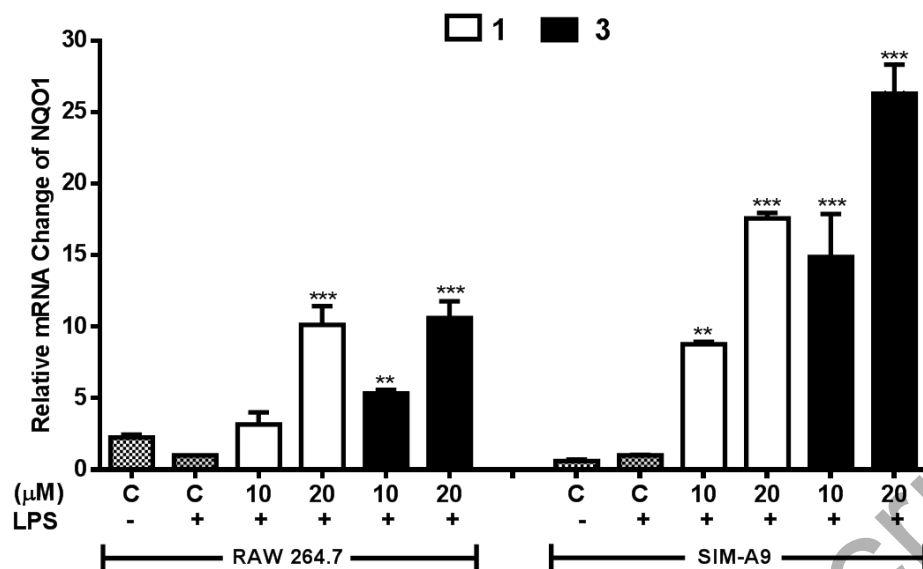


**Figure 10.** Effect of **1** and **3** on NQO1 mRNA expression in LPS induced RAW 264.7 macrophage cells and SIM-A9 microglia cells. The cells were treated with LPS (except for negative control-C) and 5,10 and 20 μM doses of the **1** and **3**. The figures show the mean results of the triplicate experiment. C: Control. Each bar represents the mean ±SEM, \*\*p<0.05, \*\*\*p<0.001.

In terms of hemeoxygenase (HO-1), compounds **1** and **3** did not result in similar positive effects. 1 μg/mL LPS treatment caused a slight upregulation (around 4 fold) at the mRNA level of HO-1 in both macrophage and microglia cells as reported in previous research studies where LPS above 100ng/mL concentration significantly induces expression of this enzyme (Figure 11) (Ye, Wang et al. 2014). On the other hand, treatment with both compounds **1** and **3** resulted in repression of the mRNA expression to a similar level, which was observed in non-treated control cells. HO-1 catalyzes the degradation of heme groups to carbon monoxide (CO), free ferrous iron (Fe<sup>2+</sup>) and biliverdin. By the action of biliverdin reductase, the latter product is metabolized to bilirubin which can remove hydroxyl radicals, superoxide anions, and singlet oxygen. Bilirubin also prevents protein and lipid peroxidation as well as exhibits strong antioxidant, anti-apoptotic and anti-inflammatory functions. Therefore, HO-1 indirectly exerts cytoprotection through the biological activities of its downstream products. Different studies on microglial and macrophage cells demonstrated that upregulation of HO-1

has a strong anti-inflammatory effect. This has been evidenced both in cell cultures and animal models treated with different pharmacological agents as well as natural compounds able to activate Nrf2/HO-1 (Tumer, Yılmaz et al. 2018). However, opposite evidences are also available such as decreasing neuroprotective effects of epigallocatechin-3-gallate and glatiramer acetate by upregulation of HO-1 in experimental autoimmune encephalomyelitis model (Janssen, Fiebiger et al. 2015). Moreover, it is also well established that HO-1 is overexpressed in the brains of patients with AD, particularly in the hippocampus and cerebral cortex region, as well as in nigralastroglia and in dopaminergic neuronal Lewy bodies of PD patients. This up-regulation has been linked to the late phase of neurodegeneration and has been proposed as biomarker of AD and PD (Nitti, Piras et al. 2018).

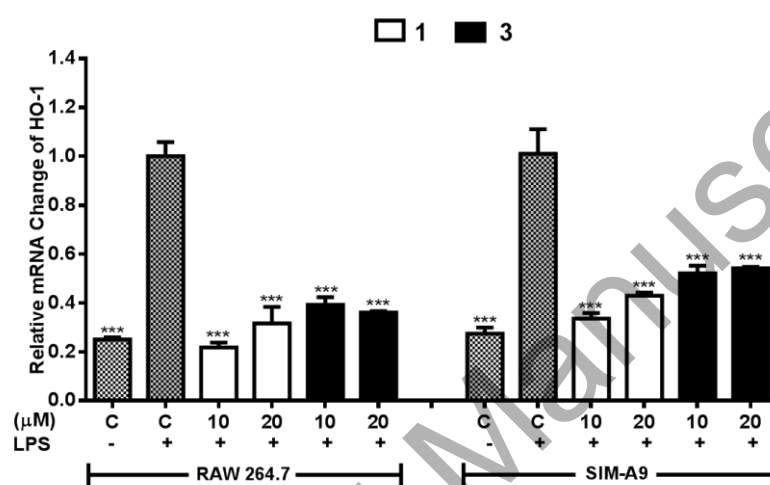


**Figure 11.** Effect of **1** and **3** on HO-1 mRNA expression in LPS induced RAW 264.7 macrophage cells and SIM-A9 microglia cells. The cells were treated with LPS (except for negative control-C) and 5,10 and 20  $\mu$ M doses of the **1** and **3**. The figures show the mean results of the triplicate experiment. C: Control. Each bar represents the mean  $\pm$ SEM, \*\* $p < 0.05$ , \*\*\* $p < 0.001$ .

Although the role played by HO-1 in oxidative stress and neuroinflammation is highly complex and is not completely understood due to contradictory results obtained, it has been recently postulated that upregulation of HO-1 in glial compartment of the brain may promote bioenergetics failure by affecting iron metabolism and mitochondrial activity (Nitti, Piras et al. 2018). In fact, it is proposed that the dysregulation of heme degradation pathway through the alteration of iron metabolism and the mitochondrial impairment may lead to neurodegeneration not only when it occurs in glial cells, but also in neurons (Nitti, Piras et al. 2018). When the intensity and duration of HO-1 up-regulation increase beyond a level this

may increase tissue damage mainly through heme-derived iron, which favors oxidative stress in mitochondria and other compartments (Nitti, Piras et al. 2018). In this aspect, the smoothing effect of compound **1** and **3** on the expression of HO-1 may be the advantages of these compounds in case of long term uses if they can be developed as potential neuroprotective lead compounds. However, more studies are warranted in this aspect.

### The effect of compound **1** and **3** on nuclear accumulation of Nrf2 protein.

Although both **1** and **3** resulted in substantial elevation in the mRNA expression of Nrf2, nuclear accumulation of this protein is essential for its function as transcription factor for activating Nrf2-ARE pathway. Some activators might promote the release of Nrf2 from its inhibitor Keap1 resulting in increased level of Nrf2 in nucleus. In the present work, as shown by Figure 12, **1** at 5, 10 and 20  $\mu$ M increased the accumulation of Nrf2 protein to nuclear region in a dose dependent manner 1.7, 1.9 and 5.1-fold, respectively as compared control group. Treatment with **3**, resulted in a more prominent effect, 2.1, 3.1 and 7.1-fold increases at 5, 10 and 20  $\mu$ M doses, respectively when compared to control group. Protein results together with those obtained from mRNA expression studies may indicate that **1** and **3** regulate Nrf2 expression at both transcriptional and posttranscriptional level. It has been evidenced that therapeutic compounds such as chemopreventive agents disorder Keap1-Nrf2 PPI by direct binding to Keap1 pocket to where the 16-mer peptide of Neh2 domain of Nrf2 binds. To investigate whether compound **1** and **3** activate Nrf2 by disrupting PPI, we performed in silico analyses.

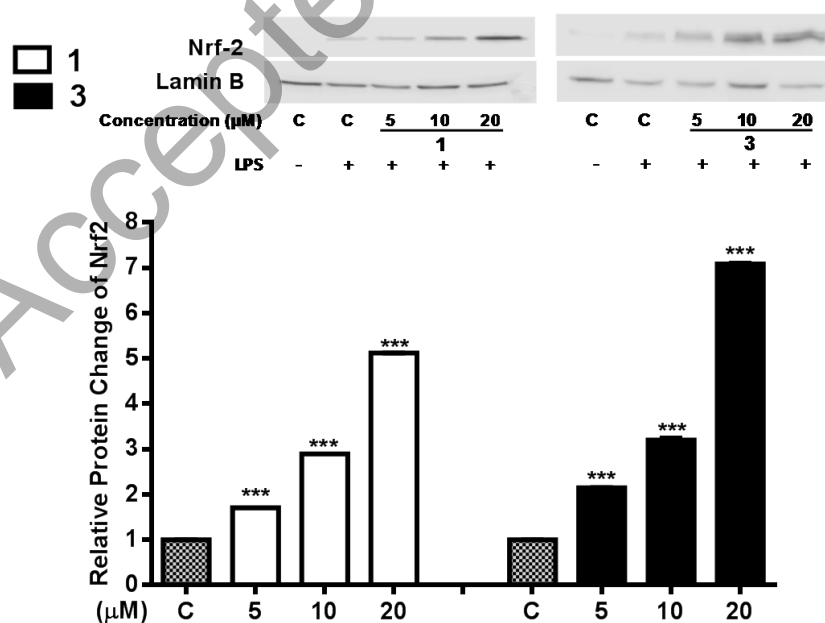


**Figure 12.** Effect of **1** and **3** on Nrf2 protein expression in LPS induced RAW 264.7 macrophage cells. The cells were treated with LPS and 5, 10 and 20  $\mu$ M doses of the **1** and **3**. The figures show the mean results of the triplicate experiment. C: Control. Each bar represents the mean  $\pm$ SEM, \*\* $p < 0.05$ , \*\*\* $p < 0.001$ .

### ***In Silico* Investigation of Studied Compounds at the Binding Pocket of Keap1.**

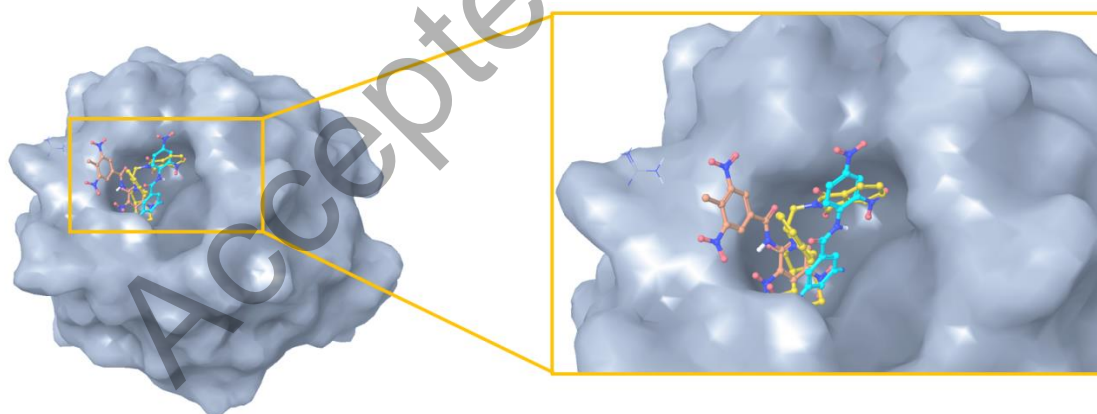
In order to understand the molecular mechanisms of studied molecules at the interactions of Keap1, these molecules were docked to the Keap1 target. Results showed that compounds **1** and **3** have higher docking scores at the binding pocket compared to other nitro derivatives (Table S2 of the Supporting Information). 2D and 3D ligand interactions diagrams of compounds **1** and **3** which shows top-docking poses has been represented at the Figure 13. These interactions were also compared with a well-known Keap1 Nrf2 PPI inhibitor LH601A. Although compounds **1** and **3** have common binding interactions, their bioactive conformations at the Keap1 was slightly different. While crucial salt bridge and hydrogen bonding interactions were constructed with Arg380, Ser363, Asn414, Arg415 and Tyr525 with compound **1**, corresponding interactions were Arg380, Asn382, Tyr334 and Tyr572 in compound **3**. Positive control molecule was constructed similar interactions (i.e., Arg380, Asn382 and Tyr525).

Current work represented herein has shown that both compounds **1** and **3** might be promising hits and represent highly promising starting point for the development of potent neuroprotective agents against neurodegenerative diseases. In this aspect, further studies including *in silico* target based structural optimization of these two compounds and also validation of their potency by *in vitro* and *in vivo* models will be crucial. However, it is well known that numerous lead compounds have failed in animal studies and clinical trials due to issues related with ADME and toxicity. For this reason, in the present study we evaluated both compounds in terms of pharmacokinetic and toxicity parameters by using *in silico* techniques.

### **Pharmacokinetic and Toxicity Predictions of Compounds 1 and 3**

Identification of novel compounds against neurodegenerative diseases are hot topics of both academy and industry, however, these compounds face various challenges such as specificity and potential toxicities as they may interfere with other pathways and cellular processes

regulated by iNOS or Keap1. For this reason, we have decided to evaluate chemical properties, possible metabolites, potential therapeutic values and toxicities of selected potent ligands. This allowed us to get a thorough understanding and prediction of their biological activity when compared to hundreds of other drugs using MetaCore from Clarivate Analytics. Toxicity properties of **1** and **3** were studied with 26-different toxicity QSAR models. (Table S3 of the Supporting Information) Compound **3** did not show significant high toxicity profiles except the AMES model. Compound **3** showed no toxicity predictions in 18 toxicity QSAR models and it showed slightly larger values in 7 toxicity QSAR models than the threshold values. Compound **1** showed no toxicity predictions in 13 toxicity QSAR models and in slightly larger toxicity predictions in 5 QSAR models. It shows high risks for following toxicity models: AMES, Anemia, Carcinogenicity (both in mouse female and rat male models), hepatotoxicity, liver necrosis, and in liver weight gain models. (Table S3 of the Supporting Information) When ADME and protein binding QSAR models were investigated with both compounds **1** and **3**, it is found that both compounds can permeate in BBB penetration model. (Table S4 of the Supporting Information) In the Table, the data is expressed as log values of the ratio of the metabolite concentrations in brain and plasma. Cutoff is -0.3 and larger values indicate that the metabolite is more likely to enter the brain. Both compounds have desired lipophilicity values. Although both compounds have higher affinity to human serum albumin, their retention time (i.e., the model is based on retention times of compounds assayed by HPLC using an immobilized HSA column) is low.





In conclusion, in the current work we showed that the compounds 3,5-dinitro-*N*-(2,4-dinitrophenyl)benzamide (**1**) and 4-methyl-3,5-dinitro-*N*-(2,4-dinitrophenyl)benzamide (**3**) display marked inhibitory potential on NO/iNOS signaling as well as potent activator properties on Nrf2 and associated cytoprotective enzymes in LPS-stimulated macrophages and microglial cells. It is evident from our current and previous work that when the nitro groups exist at the -2,4 and -3,5 positions on the phenyl ring, the activity of the substituted aromatic amide compounds increasing due to their better electron withdrawing properties and mesomeric effects at the binding pocket of the target structures. Molecular docking, MD simulations and ADMET analysis also presented that both compound **1** and **3** can be classified as druggable molecule in drug design. Therefore, nitrobenzamide scaffolds may represent a promising template and starting point, which may lead to novel small molecules to manage neuroinflammatory diseases.

## **AUTHOR INFORMATION**

### **Author contributions**

T.B.T. designed the project, supervised all contributions, wrote and finalized the draft manuscript. F.C.O. and M.A. synthesized the compounds wrote the draft of the relative section. S.S.K., Y.B.Y. and A.O. performed bioactivity studies, assisted data analysis, and construction of figures/ tables of the related parts. S.D. and K.S. conceived and performed the molecular modeling/ADMET studies and wrote the draft of the relative sections. All authors read and approved the final manuscript.

### **Conflict of interest**

We have no conflict of interest whether of a financial or other nature.

### **Acknowledgements**

Synthesis part of this study was partially supported by a research grant from the Scientific and Technological Research Council of Turkey-TUBITAK (Grant No. 110T754).

## References

- Gill, E. L., S. Raman, R. A. Yost, T. J. Garrett and V. Vedam-Mai (2018). "l-Carnitine Inhibits Lipopolysaccharide-Induced Nitric Oxide Production of SIM-A9 Microglia Cells." ACS chemical neuroscience **9**(5): 901-905.
- Güngör, T., F. C. Önder, E. Tokay, Ü. G. Gülhan, N. Hacıoğlu, T. T. Tok, A. Çelik, F. Köçkar and M. Ay (2019). "Prodrugs for nitroreductase based cancer therapy-2 novel amide/Ntr combinations targeting PC3 cancer cells." European Journal of Medicinal Chemistry.
- Janssen, A., S. Fiebiger, H. Bros, L. Hertwig, S. Romero-Suarez, I. Hamann, C. Chanvillard, J. Bellmann-Strobl, F. Paul and J. M. Millward (2015). "Treatment of chronic experimental autoimmune encephalomyelitis with epigallocatechin-3-gallate and glatiramer acetate alters expression of heme-oxygenase-1." PLoS One **10**(6): e0130251.
- Kanan, T., D. Kanan, I. Erol, S. Yazdi, M. Stein and S. Durdagi (2019). "Targeting the NF- $\kappa$ B/I $\kappa$ B $\alpha$  complex via fragment-based E-Pharmacophore virtual screening and binary QSAR models." Journal of Molecular Graphics and Modelling **86**: 264-277.
- Nagamoto-Combs, K., J. Kulas and C. K. Combs (2014). "A novel cell line from spontaneously immortalized murine microglia." Journal of neuroscience methods **233**: 187-198.
- Nitti, M., S. Piras, L. Brondolo, U. Marinari, M. Pronzato and A. Furfaro (2018). "Heme Oxygenase 1 in the Nervous System: Does It Favor Neuronal Cell Survival or Induce Neurodegeneration?" International journal of molecular sciences **19**(8): 2260.
- Samaradivakara, S. P., R. Samarasekera, S. M. Handunnetti, O. J. Weerasena, A. A. Al-Hamashi, J. T. Slama, W. R. Taylor, Q. Alhadidi, Z. A. Shah and L. Perera (2018). "A Bioactive Resveratrol Trimer from the Stem Bark of the Sri Lankan Endemic Plant *Vateria copallifera*." Journal of natural products **81**(8): 1693-1700.
- Shityakov, S., N. Roewer, C. Förster and J.-A. Broscheit (2017). "In silico investigation of propofol binding sites in human serum albumin using explicit and implicit solvation models." Computational biology and chemistry **70**: 191-197.
- Shityakov, S., T. Sohajda, I. Puskás, N. Roewer, C. Förster and J.-A. Broscheit (2014). "Ionization states, cellular toxicity and molecular modeling studies of midazolam complexed with trimethyl- $\beta$ -cyclodextrin." Molecules **19**(10): 16861-16876.
- Steinert, J. R., T. Chernova and I. D. Forsythe (2010). "Nitric oxide signaling in brain function, dysfunction, and dementia." The Neuroscientist **16**(4): 435-452.
- Thiel, V. E. and K. L. Audus (2001). "Nitric oxide and blood-brain barrier integrity." Antioxidants and Redox Signaling **3**(2): 273-278.
- Tse, J. K. (2017). "Gut microbiota, nitric oxide, and microglia as prerequisites for neurodegenerative disorders." ACS chemical neuroscience **8**(7): 1438-1447.
- Tumer, T. B., F. C. Onder, H. Ipek, T. Gungor, S. Savranoglu, T. T. Tok, A. Celik and M. Ay (2017). "Biological evaluation and molecular docking studies of nitro benzamide derivatives with respect to in vitro anti-inflammatory activity." International immunopharmacology **43**: 129-139.
- Tumer, T. B., B. Yılmaz, A. Ozleyen, B. Kurt, T. T. Tok, K. M. Taskin and S. S. Kulabas (2018). "GR24, a synthetic analog of Strigolactones, alleviates inflammation and promotes Nrf2 cytoprotective response: In vitro and in silico evidences." Computational biology and chemistry **76**: 179-190.
- Ye, M., Q. Wang, W. Zhang, Z. Li, Y. Wang and R. Hu (2014). "Oroxylin A exerts anti-inflammatory activity on lipopolysaccharide-induced mouse macrophage via Nrf2/ARE activation." Biochemistry and Cell Biology **92**(5): 337-348.